Autoantigen Tetramer Silences Autoreactive B Cell Populations

Matthew A. Christopher[1,*], **Stephanie N. Johnson**[1,*], **J. Daniel Griffin**[1,2], **Cory Berkland**[1,2,3,**]

[1]Department of Pharmaceutical Chemistry, University of Kansas, 2095 Constant Avenue, Lawrence, Kansas 66047, USA

[2]Bioengineering Graduate Program, University of Kansas, 1520 West 15th Street, Lawrence, KS 66045, USA

[3]Department of Chemical and Petroleum Engineering, University of Kansas, 1530 West 15th Street, Lawrence, KS 66045, USA

Abstract

Many autoimmune therapies focus on immune suppression to reduce symptom severity and halt disease progression; however, currently approved treatments lack specificity for the autoantigen and rely on more global immune suppression. Multivalent antigen arrays can disarm pathogenic autoimmune B cell populations that specifically recognize the antigen of interest via their B cell receptor (BCR). Disarmament may be achieved by BCR engagement, crosslinking, and sustained receptor occupancy as a result of multivalent, high avidity BCR binding. To engage and explore this mechanism, a tetramer display of the encephalogenic proteolipid peptide (PLP$_{139-151}$), referred to as 4-arm PLP$_{139-151}$, was synthesized by copper-catalyzed azide-alkyne cycloaddition chemistry. Subcutaneous administration of 4-arm PLP$_{139-151}$ completely ameliorated symptoms of paralysis in a mouse model of multiple sclerosis known as experimental autoimmune encephalomyelitis. Competitive binding of 4-arm PLP$_{139-151}$ to PLP$_{139-151}$-specific IgG in mouse serum demonstrated the enhanced avidity associated with the multivalent array compared to free peptide. Furthermore, key PLP$_{139-151}$-reactive B cells were depleted following 4-arm PLP$_{139-151}$ treatment, resulting in significant reduction of pro-inflammatory cytokines. Together, these data demonstrate the potential of 4-arm PLP$_{139-151}$ to silence autoreactive B cell populations and limit downstream activation of effector cells.

Graphical Abstract

[**]To whom correspondence should be addressed: University of Kansas, 2030 Becker Drive, Lawrence, KS 66047., Phone: (785) 864-1455, Fax: (785) 864-1454, berkland@ku.edu.
[*]These authors contributed equally to this work.

[7.]Supporting Information

Figure S1. SEC chromatograms of PEG standards. Figure S2. PLP$_{139-151}$-specific IgG antibody titers in EAE mouse serum. Figure S3. Flow cytometric analysis of surface receptor expression in EAE splenocytes following *in vitro* treatment. Figure S4. Flow cytometric analysis of CD80 and CD86 expression in EAE splenocytes following *in vitro* treatment. Figure S5. ELISA analysis of cytokine expression of EAE splenocytes following *in vitro* treatment. Figure S6. Representative flow cytometric analysis displaying gating schemes for each fluorescent channel. Figure S7. Representative flow cytometric plots displaying changes in CD19 expression following treatment.
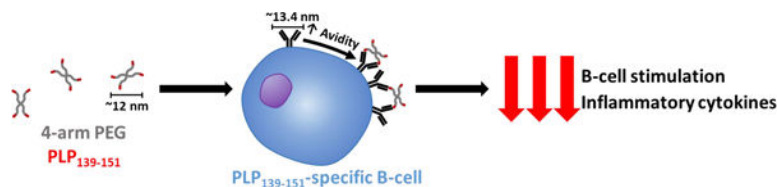
1. Introduction

Autoimmunity is characterized by a loss of immune tolerance toward self-antigens resulting in aberrant inflammatory events.[1–2] Typical treatments for autoimmune diseases lack specificity for the offending, autoreactive T cells and B cells, which can induce a wide range of adverse side effects. Many such autoimmune therapies induce global immune suppression, hindering the immune system's ability to eliminate pathogens.[3] This immune suppression may relieve autoimmune symptoms, but it also leaves the patient susceptible to opportunistic infections. There is a crucial need for antigen-specific immunotherapies (ASITs) capable of inducing immune tolerance toward an autoantigen without compromising immune function.

In multiple sclerosis (MS), loss of immune tolerance toward myelin sheath autoantigens results in abnormal inflammatory responses in the central nervous system facilitated by both autoreactive T cells and B cells.[4–5] The result of this inflammation is demyelination and neuronal degradation leading to neurological dysfunction.[6] The role of B cells in MS pathology is still unclear, however, the success of B cell depletion in clinical studies utilizing Rituximab, an anti-CD20 mAb, suggests autoreactive B cells function beyond autoantibody secretion.[7–10] MS patients who received Rituximab exhibited improvement in disease progression, even though they maintained high serum levels of autoantibodies against myelin antigens. These results indicated antibody-independent mechanisms for B cell involvement in MS, including antigen presentation to T cells and B cell cytokine and chemokine production.[7] The successes of B cell depletion therapies in MS patients implicate autoreactive B cells as an excellent target for tolerance induction through ASITs. Autoreactive B cells may be targetable through their high-affinity membrane bound B cell receptor (BCR) specific for MS autoantigens.

Polymers with grafted antigens have been shown to specifically target and disarm B cells driving autoimmunity. Beginning in the 1970s, Dintzis and colleagues investigated polymers grafted with haptens (small molecule antigens) to induce antigen-specific B cell responses. The solubility, molecular weight of the polymer backbone, polymer type, and antigen valency were systematically varied and B cell responses observed.[11] Interestingly, their findings revealed that large (>100 kDa) polymer backbones with increased antigen valency elicited an immunogenic response; however, smaller antigen arrays (<100 kDa) and lower valency arrays invoked long-term immune tolerance to the hapten (antigen). Additionally,

based on their greater molecular weight in comparison to peptide antigen, multivalent arrays may also impart pharmacokinetic advantages regarding biotherapeutic distribution. Namely, following subcutaneous administration, drug absorption into the lymphatic system is increased with increasing molecular weight for therapeutics greater than 16 kDa and less than 150 kDa; a feature which may improve the exposure of multivalent arrays to target B cell populations in lymph nodes as compared to free peptide antigens.[12–13] In more recent work, Dintzis and others demonstrated the potential for antigen arrays <100 kDa to selectively eliminate high affinity B cells specific for the antigen of interest.[14] Our lab has investigated this phenomenon and determined BCR crosslinking and sustained receptor occupancy induced by antigen arrays may selectively target and disarm autoreactive B cells.[15–17]

Building upon these findings, our lab has developed a framework for multivalent antigen presentation known as soluble antigen arrays (SAgAs) and investigated their tolerogenic effects in a mouse model of MS known as experimental autoimmune encephalomyelitis (EAE).[18] SAgAs are a multivalent array of MS autoantigen proteolipid protein ($PLP_{139–151}$) with or without a cell adhesion inhibitor peptide (LABL) presented on a polymeric backbone of hyaluronic acid. SAgAs were shown to act in an antigen-specific manner and facilitate BCR crosslinking in B cells.[19] These studies demonstrated potential therapeutic efficacy in the treatment of MS, prompting further exploration of PLP-specific multivalent array structures capable of engaging BCRs on the surface of B cells.

Herein, we outline the synthesis and characterization of a novel polymeric array of $PLP_{139–151}$ for use in the EAE model of MS. This multivalent antigen array, referred to as 4-arm $PLP_{139–151}$, consists of a 20 kDa polyethylene glycol (PEG) tetramer backbone with the $PLP_{139–151}$ peptide epitope conjugated to each terminus. This structure offers control over the number and positioning of reactive sites, a simple synthetic process, and homogenous product. The efficacy of 4-arm $PLP_{139–151}$ was demonstrated *in vivo* through a 25-day EAE study. Additionally, the immune mechanisms associated with 4-arm $PLP_{139–151}$ treatment in splenocytes were explored through cell phenotyping using flow cytometry, co-stimulatory marker expression, and downstream effector cell responses gauged by quantification of inflammatory cytokine expression following treatment.

2. Experimental Section

Materials

20 kDa 4-arm PEG-azide was purchased from JenKem Technology USA (Beijing, China). Tris(3-hydroxypropyltriazolylmethyl)amine (THPTA) and sodium ascorbate (NaAsc) were purchased from Sigma-Aldrich (St. Louis, MO). Copper (II) sulfate pentahydrate ($CuSO_4 \bullet 5 H_2O$) was purchased from Acros Organics (Geel, Belgium). Alkyne functionalized peptide bearing an *N*-terminal 4-pentynoic acid (homopropargyl, hp) modification, $hpPLP_{139–151}$ (hp-HSLGKWLGHPDKF-OH), was obtained from Biomatik, USA, LLC (Wilmington, DE). All reagents were used as received without further purification. For *in vitro* cell assays and *in vivo* studies, female 4–6-week-old SJL/J (H-2) mice were purchased from Envigo Laboratories (Indianapolis, IN). For EAE induction, incomplete Freund's adjuvant (IFA) and heat-killed mycobacterium tuberculosis H37RA were purchased from Difco (Sparks, MD).

Additionally, pertussis toxin was purchased from List Biological Laboratories (Campbell, CA). For use in flow cytometry, TruStain fcX (anti-mouse CD16/32), R-phycoerythrin (PE)/Cy7-conjugated anti-mouse CD3, PE-conjugated anti-mouse CD86, FITC-conjugated anti-mouse CD80, AlexaFluor647-conjugated anti-mouse CD19, and BV421-conjugated anti-mouse CD11c were purchased from BioLegend (San Diego, CA).

Synthesis of 4-arm $PLP_{139-151}$

4-arm $PLP_{139-151}$ was synthesized by copper-catalyzed azide-alkyne cycloaddition (CuAAC) chemistry, as shown in Scheme 1. First, $hpPLP_{139-151}$ (43 μmol) was added to a 20 mL scintillation vial with a stir bar. The powder was then dissolved in 5 mL of 50 mM phosphate buffer (pH 7.4) at room temperature. A 10 mM solution of 20 kDa 4-arm PEG-azide (10 μmol) in DMSO was then added to the solution, followed by a 120 mM solution of $CuSO_4 \bullet 5H_2O$ (120 μmol) in 50 mM phosphate buffer (pH 7.4). Then, THPTA (600 umol) was added as a 600 mM solution in 50 mM phosphate buffer (pH 7.4). A 100 μL aliquot was removed for HPLC analysis before the addition of a 1 M solution of NaAsc (2.4 mmol) in 50 mM phosphate buffer (pH 7.4). The reaction was stirred at room temperature and the extent of conjugation was monitored by HPLC at various times. Upon completion of the reaction at 24 hrs, the solution was purified by semi-preparative HPLC utilizing a linear elution gradient of acetonitrile in water (constant 0.05% trifluoroacetic acid) over 20 min, with a Waters XBridge BEH C_{18}, 5μm, 130 Å stationary phase (19 × 250 mm), with a 14.0 mL/min flow rate. The purified fraction was then concentrated under vacuum, transferred to vials, frozen, and lyophilized.

Analytical Characterization of 4-arm $PLP_{139-151}$

RP-HPLC analysis was conducted using a Waters Alliance HPLC system equipped with a dual wavelength UV/vis detector. Chromatographic conditions utilized a linear gradient from 5–95% acetonitrile in water (constant 0.05% trifluoroacetic acid) over 20 min, with a Waters XBridge C18, 5μm, 130 Å stationary phase (4.6 × 250 mm) with a 1.0 mL/min flow rate and detection at 214 nm. The followed equation was used to quantitate conjugation of $PLP_{139-151}$

$$N_{con} = \left[\left(\frac{n_{PLP139-151}}{n_{4-arm\ PEG-azide}} \right) \left(\frac{V_{pre} - V_{sam}}{V_{pre}} \right) \right] \left(1 - \frac{PA_t}{PA_{start}} \right)$$

where N_{con} = number of conjugated $PLP_{139-151}$ molecules per backbone, $n_{PLP139-151}$ = moles of $PLP_{139-151}$ used in the reaction, $n_{4-arm\ PEG-azide}$ = number of moles of 20 kDa 4-arm PEG-azide used in the reaction, V_{pre} = total reaction volume before NaAsc is added, V_{sam} = volume of "pre-NaAsc" aliquot removed from the reaction mixture, PA_t = the measure peak area of $PLP_{139-151}$ at time t, and PA_{start} = the measure peak area of $PLP_{139-151}$ before NaAsc is added to the reaction.

Nuclear magnetic resonance imaging (NMR) spectra were collected on a Bruker Avance AVIII 500 MHz spectrometer equipped with a dual carbon/proton cryoprobe, and all samples were dissolved in 600 μL D_2O for analysis. MestReNova 12.0 was used for NMR data analysis.

Size exclusion chromatography (SEC) was conducted using a Waters Alliance HPLC system equipped with a dual wavelength UV/vis detector and an RI detector. Chromatographs were collected using a Waters XBridge® BEH 125 SEC, 2.5 μm, 125 Å stationary phase (7.8 × 300 mm) column at a flow rate of 0.5 ml/min over 60 minutes using saline as a mobile phase. The PEG standards were detected by the RI detector and 4-arm PEG-N_3 and 4-arm $PLP_{139-151}$ was analyzed at 214 nm.

Dynamic Light Scattering (DLS) was performed using a DynaPro Plate Reader (Wyatt Technology, Santa Barbara, CA). Incident light was detected in a backscattering configuration and analyzed with an autocorrelator. Sample (20 μL), in DI water, was placed in a clear-bottomed 384-well plate and read at 20 °C. Samples were measured 5 times with a 15 s acquisition time. Autocorrelation functions were fit using cumulant analysis, and intensity averaged values are reported. Errors are reported as standard deviation of 3 replicates.

Matrix-assisted laser desorption/ionization-time of flight (MALDI-TOF) mass spectrometry (MS) was completed by spotting samples with α-Cyano-4-hydroxycinnamic acid matrix solution prior to analysis on a Bruker Autoflex MAX MALDI mass spectrometer. FlexControl 3.4 was utilized to analyze the data.

Induction of EAE

In vivo efficacy and *in vitro* cell assays were performed through induction of EAE in female 4–6-week-old SJL/J (H-2) mice. All protocols were approved through the University's Institutional Animal Care and Use Committee with animals housed in pathogen-free conditions. Induction of EAE was carried out using an emulsion of 200 μg free $PLP_{139-151}$ in PBS emulsified with Complete Freund's Adjuvant (CFA) containing 4 mg/mL heat-killed *M. Tuberculosis* strain H37RA. This emulsion was administered subcutaneously to mice on day 0 in 50 μL injections above each shoulder and hind flank for a total injection volume of 200 μL per mouse. At this time, 100 μL intraperitoneal injections of pertussis toxin at 100 ng/mL in PBS were administered to the mice. The administration of pertussis toxin was also repeated on day 2. Beginning on day 7, severity of disease symptoms was recorded daily using the following clinical scoring system: 0, no clinical disease symptoms; 1, weakness or limpness of the tail; 2, weakness or partial paralysis of one or two hind limbs (paraparesis); 3, full paralysis of both hind limbs (paraplegia); 4, paraplegia plus weakness or paralysis of forelimbs; 5, moribund (euthanasia necessary). Mouse body weight was recorded daily throughout the entire study.

Competitive $PLP_{139-151}$ ELISA

Competitive binding of 4-arm $PLP_{139-151}$ to EAE serum antibodies was detected using an indirect ELISA. Initially, 100 μL of 1 mg/mL free $PLP_{139-151}$ at pH 9.5 (50 mM sodium bicarbonate buffer) was incubated overnight in an Immulon 2HB plate at 4°C. Wash buffer consisting of 1x Phosphate Buffered Saline (PBS) with 0.5% Tween 20 was used to wash the plate 3 times with 300 μL/well. Block buffer was prepared using 0.2 μm filtered PBS containing 1% Bovine Serum Albumin (BSA). The plate was blocked with 250 μL of block buffer incubated at 37°C for 1 hour. Serum samples obtained from EAE mice at peak of

disease severity were thawed and pre-incubated with one of the following treatments: 4-arm $PLP_{139-151}$, 20 kDa 4-arm PEG-azide, free $PLP_{139-151}$, or PBS. These treatments were maintained at 25 μM $PLP_{139-151}$ basis and were incubated with the serum for 1 hour. Once again, the plate was washed 3 times with wash buffer, as described previously. Treated serum samples were added to the plate and serially diluted in reagent diluent consisting of 1% BSA and 0.5% Tween 20 in 1x PBS. Samples were incubated in the plate for 1 hour at 37°C. The plate was washed 3 times with wash buffer, as described previously. Secondary antibody solution was prepared using anti-mouse IgG diluted in reagent diluent. Each well was incubated with 100 μL of secondary antibody solution for 1 hour at 37°C. The plate was washed 3 times with wash buffer and 100 μL of TMB solution was added to each well. The plate was shaken at 200 rpm for 15 minutes prior to the addition of 100 μL/well of 2N sulfuric acid to quench the reaction. Lastly, the absorbance at 450/540 nm was read on a Spectramax M5 (Molecular Devices) plate reader.

In Vivo Efficacy

Treatment efficacy *in vivo* was determined using 6 mice per group. All mice were euthanized after 25 days. Treatments were subcutaneously administered on the back of the neck in 100 μL of 40 mg/mL. Each group was dosed on a 200 nmol $PLP_{139-151}$ basis, with doses administered on days 4, 7, and 10 following EAE induction. Mouse weights were recorded daily beginning on day 0 and clinical scores were recorded daily beginning on day 7.

Splenocyte Isolation

Spleens were isolated from EAE mice at peak of disease for *in vitro* studies. Spleens were placed on ice in 5 mL of RPMI 1640 containing L-glutamine and 1% Penicillin-Streptomycin. Cellular extract was collected by pressing the spleens into a wire mesh using the plunger of a 1 mL syringe. The extract was centrifuged at 1100 xg for 5 minutes and resuspended in red blood cell lysis solution at room temperature for 5 minutes. The lysis solution was quenched through the addition of cold RPMI 1640 supplemented with L-glutamine, 1% Penicillin-Streptomycin, and 10% fetal bovine serum (FBS) (complete RPMI, cRPMI). The cells were then centrifuged at 1100 xg for 5 minutes and resuspended in cRPMI for counting in 0.04% trypan blue. Cells were counted using a Nexcelom Bioscience Cellometer Auto T4. *In vitro* cell incubation was carried out at 37°C and 5% CO_2 for 72 hours following addition of treatment.

Cell Staining for Flow Cytometry

EAE splenocytes were incubated at 5×10^6 cells/well in a 24 well plate at a final volume of 1 mL. Treatments were added on a 25 μM $PLP_{139-151}$ basis, and $PLP_{139-151}$ rechallenge consisted of the addition of 25 μM free $PLP_{139-151}$ to the well. Following 72 hours incubation with treatment, a portion of cell supernatant was removed for future processing and the remaining cells were washed with RPMI + 5% FBS and centrifuged. Cells were resuspended in 50 μL of 20 μg/mL TruStain fcX and placed on ice for 30 minutes. Next, 50 μL of antibody solution was added, according to manufacturer recommendations, and the solution was kept on ice for 1 hour. Antibody stains included: R-phycoerythrin (PE)/Cy7-conjugated anti-mouse CD3, PE-conjugated anti-mouse CD86, FITC-conjugated anti-mouse

CD80, AlexaFluor647-conjugated anti-mouse CD19, and BV421-conjugated anti-mouse CD11c. Sample data was collected using a BD FACSFusion Cytometer with 30,000 events per sample. Sample data was analyzed using Kaluza and GraphPad Prism.

Cytokine Measurement

Prior to sample processing for flow cytometry, cell supernatant was removed from the samples. This supernatant was frozen at −80°C until cytokine analysis could be carried out. The secretion of IFN-γ, TNF-α, GM-CSF, IL-2, IL-6, IL-10, IL-12p70, IL-15, IL-17A, and IL-23 was detected using a U-Plex kit while following manufacturer instructions (Meso Scale Discovery).

Statistical Analysis

Statistical analysis in all assays was carried out using two-way analysis of variance (ANOVA) and Tukey multiple comparisons tests. Criteria for significance in cytokine analysis are as follows: * $p < 0.05$, ** $p < 0.01$, *** $p < 0.001$, **** $p < 0.0001$. For cytometry samples * represents significance ($p < 0.05$ or better) from the 4-arm $PLP_{139-151}$ treatment group with 25 μM $PLP_{139-151}$ rechallenge. Additionally, for flow cytometry samples # represents significance ($p < 0.05$ or better) from the 4-arm $PLP_{139-151}$ treatment group with no $PLP_{139-151}$ rechallenge. All statistical analysis was performed using GraphPad Prism.

3. Results

Synthesis and Analytical Characterization of 4-arm $PLP_{139-151}$

The 4-arm $PLP_{139-151}$, with an average of 3.3 $PLP_{139-151}$ molecules per polymer, was synthesized by conjugating multiple modified autoantigen ($hpPLP_{139-151}$) molecules to 20 kDa 4-arm PEG-azide. Both qualitative and quantitative analytical techniques were used to characterize 4-arm $PLP_{139-151}$ and its components. $^1H/^{13}C$ Heteronuclear Single Quantum Coherence (HSQC) NMR spectroscopy was used to confirm successful conjugation. The spectra of 20 kDa 4-arm PEG-azide showed one major resonance corresponding to the PEG backbone (Figure 1A). The unique resonance signal for the terminal alkyne of the homopropargyl linker on $hpPLP_{139-151}$ ($\delta(^1H) \approx 2.6$ ppm, $\delta(^{13}C) \approx 70$ ppm) was clearly evident (Figure 1B). However, following conjugation, this resonance signal was absent (Figure 1C), indicating that 4-arm $PLP_{139-151}$ contained only the conjugated peptide. Further, the incorporation of both components into the final product was observed by comparing the individual resonances from 20 kDa 4-arm PEG-azide (Figure 1A) and $hpPLP_{139-151}$ (Figure 1B), to the HSQC spectrum of 4-arm $PLP_{139-151}$ (Figure 1C).

In order to gain information regarding the size of the tetramer, SEC, DLS, and MALDI-TOF data were collected. Results from SEC revealed molecular weights of 26,940 Da and 28,940 Da for 4-arm PEG-N3 and 4-arm $PLP_{139-151}$, respectively. DLS data estimated the hydrodynamic radius of 1.67 nm, and 1.75 nm for 20 kDa 4-arm PEG-N_3, and 4-arm $PLP_{139-151}$, respectively. Finally, MALDI-TOF MS provided molecular weight determinations for the tetramer. Results showed that the average molecular weight of 20 kDa 4-arm PEG-N_3 and 4-arm $PLP_{139-151}$ were 20,367.485 Da and 23,758.924 Da, respectively. This change in molecular weight corresponds to the addition of 2.2 $PLP_{139-151}$ molecules on

the PEG backbone. The disagreement between the number of PLP molecules on the backbone likely results from the difficulty in accurately determining molecular weights of heterogeneous samples.

Competitive ELISA Demonstrating PLP$_{139-151}$ Specificity

Serum from EAE mice was pre-incubated with 4-arm PLP$_{139-151}$, 20 kDa 4-arm PEG-azide, or free PLP$_{139-151}$ prior to addition to a PLP$_{139-151}$-coated ELISA plate. The result of this pre-incubation was the loss of signal due to PLP$_{139-151}$-specific antibodies binding during pre-incubation. As seen in Figure 2, pre-incubation with 4-arm PLP$_{139-151}$ greatly reduced the signal in the competitive ELISA assay compared to pre-incubation with PBS, indicating that PLP$_{139-151}$-specific antibody binding sites were occupied following 4-arm PLP$_{139-151}$ pre-incubation. The 4-arm PLP$_{139-151}$ was more effective at occupying the binding sites of PLP$_{139-151}$-specific antibodies from EAE serum, compared to equimolar concentrations of free PLP$_{139-151}$. Additionally, pre-incubation with 20 kDa 4-arm PEG-azide showed some reduction of the ELISA signal, suggesting free azides may introduce some degree of non-specific binding to serum antibodies (Figure S2).

In Vivo Efficacy of 4-arm PLP$_{139-151}$

In vivo studies of 4-arm PLP$_{139-151}$ in the EAE mouse model were conducted using subcutaneous injection of treatments in 40 mg/mL mannitol at equimolar PLP$_{139-151}$ concentrations of 200 nmol. Treatments were administered on days 4, 7, and 10 with mice being observed for 25 days. Clinical scores were assigned based on disease severity, with higher scores representing more severe symptoms. Treatment with 4-arm PLP$_{139-151}$ proved most effective at eliminating EAE symptoms, as mice treated with 4-arm PLP$_{139-151}$ displayed no signs of paralysis (Figure 3). Treatment with 4-arm PLP$_{139-151}$ presented a drastic change from the control treatments, which both developed symptoms of paralysis. Furthermore, the mouse weight data (Figure 4) paralleled the clinical score data, with the 4-arm PLP$_{139-151}$ treated mice maintaining a healthy and stable weight gain throughout the study. This contrasted with the control groups, which displayed a rapid loss of weight beginning at approximately day 10.

Analysis of Key Immune Cell Populations

In vitro treatment of EAE splenocytes harvested at peak of disease with 4-arm PLP$_{139-151}$ was assessed through flow cytometric analysis of key immune cell populations. These populations included CD11c$^+$ antigen-presenting cells, CD19$^+$ B cells, and CD3$^+$ T cells. Additionally, the expression of two costimulatory markers, CD80 and CD86, was analyzed in these splenocytes. Treatment groups included media, 25 μM free PLP$_{139-151}$, 4-arm PLP$_{139-151}$, and a combination 4-arm PLP$_{139-151}$ + 25 μM free PLP$_{139-151}$. This strategy provided insight into the ability of these treatment options to suppress PLP$_{139-151}$-specific cell expansion in the presence of free, cognate antigen. Additionally, 20 kDa 4-arm PEG-azide and 20 kDa 4-arm PEG-azide + 25 μM free PLP$_{139-151}$ treatments were explored and these data are included in the supplement.

CD11c$^+$ cells represented the smallest population observed in this study, and with the inclusion of 25 μM PLP$_{139-151}$ rechallenge, the presence of this population was further

reduced through treatment with 4-arm $PLP_{139-151}$ (Figure 5). This reduction in $CD11c^+$ cells was not observed in the presence of 20 kDa 4-arm PEG-azide without conjugation of $PLP_{139-151}$. The total T cell populations remained relatively constant across all treatment options except for a small reduction in T cells when treated with 4-arm $PLP_{139-151}$ alone, compared to media alone (Figure 6).

Two populations of $CD19^+$ B cells were observed throughout this study. The first population, labeled $CD19^{+lo}$ exhibited a lower expression of CD19 on the cell surface (Figure S6). This population remained mostly constant across all treatment groups with the exception of a slight increase in $CD19^{+lo}$ cells in splenocytes treated with 4-arm $PLP_{139-151}$ + 25 μM free $PLP_{139-151}$ (Figure 5). Most interestingly, the $CD19^{+hi}$ B cell population was highly responsive to $PLP_{139-151}$-rechallenge, as the inclusion of 25 μM free $PLP_{139-151}$ resulted in marked expansion of this cell population (Figure 5). Furthermore, treatment with 4-arm $PLP_{139-151}$ nearly completely eliminated $CD19^{+hi}$ B cells from these splenocytes, both in the presence of 25 μM free $PLP_{139-151}$ and without rechallenge (Figure 5).

Costimulatory markers CD80 and CD86 were observed in EAE splenocytes following treatment, and treatment with 4-arm $PLP_{139-151}$ also had striking results on the expression of these costimulatory molecules. CD80 expression was increased following treatment with 4-arm $PLP_{139-151}$, a result that was maintained both with and without $PLP_{139-151}$ rechallenge (Figure 6A). In contrast, the expression of CD86 was significantly reduced in splenocytes treated with 4-arm $PLP_{139-151}$ (Figure 6B). The expression of CD86 was upregulated in the presence of 25 μM free $PLP_{139-151}$ in the control treatment groups, but the inclusion of 4-arm $PLP_{139-151}$ prevented this upregulation despite the presence of $PLP_{139-151}$ rechallenge (Figure 6B).

Cytokine Expression

In addition to investigating changes in key immune cell population statistics, the treated samples were also tested for differences in cytokine expression. Cytokines investigated in this assay included IFN-γ, TNF-α, GM-CSF, IL-2, IL-6, IL-10, IL-12p70, IL-15, IL-17A, and IL-23. Samples were designed for analysis in triplicate, however, GM-CSF, IL-12p70, IL-15, and IL-23 each resulted in fewer than 3 samples within the detectable range. Of the remaining cytokines, the effects of 4-arm $PLP_{139-151}$ were clear. General inflammatory cytokines such as IFN-γ (Figure 7A) and TNF-α (Figure 7B) were highly expressed in the presence of 25 μM free $PLP_{139-151}$ for control treatment groups. Despite this increase due to the presence of free $PLP_{139-151}$, 4-arm $PLP_{139-151}$ treatment prevented the increased secretion of IFN-γ (Figure 7A) and TNF-α (Figure 7B) in the presence of $PLP_{139-151}$ rechallenge. It should be noted that treatment with 20 kDa 4-arm PEG-azide in the presence of 25 μM free $PLP_{139-151}$ significantly increased the secretion of TNF-α (Figure S5B). The anti-inflammatory effects of 4-arm $PLP_{139-151}$ were also observed in expression of IL-2 (Figure 7C), where response to $PLP_{139-151}$ rechallenge was not as pronounced. IL-17A (Figure 7D) and IL-6 (Figure 7E) expression was also increased in the presence of free $PLP_{139-151}$, but treatment with 4-arm $PLP_{139-151}$ significantly reduced the secretion of both cytokines in response to $PLP_{139-151}$ rechallenge. Lastly, expression of IL-10 (Figure 7F) appeared to remain unchanged in response to the treatment groups explored in this study.

4. Discussion

Soluble multivalent antigen arrays have the potential to selectively disarm, tolerize, or delete self-reactive B cells at various stages of B cell maturity due to their high affinity interactions with the BCR, crosslinking of BCRs, and sustained receptor occupancy.[14, 20–21] As discussed above, early works in the development of multivalent arrays for tolerance induction indicated that low molecular weight antigen arrays (<100 kDa) were most effective at deactivating antigen-specific B cells, suggesting enhanced suppressive activity compared to larger constructs.[22] In studies reported here, tetramer antigen arrays (~25 kDa) displaying $PLP_{139-151}$ were investigated as a multivalent, antigen-specific therapy for inhibiting EAE induced by the $PLP_{139-151}$ epitope.

$PLP_{139-151}$ induction of EAE is known to invoke antigen-specific B and T cells responses that drive disease.[23] Adoptive transfer experiments and rechallenge studies using EAE immune cells (e.g. EAE splenocytes) have confirmed the specificity of the immune response to $PLP_{139-151}$.[24–25] Furthermore, EAE induced by $PLP_{139-151}$ has not shown immune reactivity to null antigens.[26–27] Thus, our research did not aim to reiterate the specificity of $PLP_{139-151}$ immune responses. Instead, we designed and synthesized the 4-arm $PLP_{139-151}$ for comparison to free (monovalent) $PLP_{139-151}$, ultimately showing this format change yields opposing mechanisms of disarming autoimmune B cells versus autoimmune stimulation, respectively.

The multivalent nature of 4-arm $PLP_{139-151}$ more effectively blocked $PLP_{139-151}$-specific antibodies in solution due to higher avidity; a feature resulting from the molecular design of 4-arm $PLP_{139-151}$. As seen in Figure 2, pre-incubation with 4-arm $PLP_{139-151}$ resulted in the greatest reduction of absorbance in the competitive ELISA assay. Samples pre-incubated with 4-arm $PLP_{139-151}$ displayed significantly reduced absorbance in comparison to samples pre-incubated with an equimolar amount of free $PLP_{139-151}$. Notably, the theoretical span of the 5 kDa PEG arms in 20 kDa 4-arm PEG-azide is ~6 nm.[28–29] As such, the distance between two $PLP_{139-151}$ moieties in 4-arm $PLP_{139-151}$ ranges from 8 nm to 12 nm, which is nearly identical to the spacing between the two arms of murine IgG antibody subclasses, which are reported to range from approximately 11.7 nm to 13.4 nm.[30–31] Specifically, since the $PLP_{139-151}$ multimer described herein has an average of 2.2 $PLP_{139-151}$ molecules on the PEG backbone, the distance between epitopes should be around 12 nm; whereas if all arms were occupied, lateral distances could range from ~8.5 nm between adjacent peptides for a fully occupied 4-arm structure to a maximum of ~12 nm spacing when fully stretched. Further studies utilizing various sizes of PEG backbones will need to be conducted to fully elucidate the effects of autoantigen spacing on efficacy.

In vivo treatment of EAE mice through subcutaneous injection of 4-arm $PLP_{139-151}$ prevented symptom onset in "at-risk" animals. As seen in Figure 3, subcutaneous administration of 4-arm $PLP_{139-151}$ dosed at a 200 nmol $PLP_{139-151}$ equivalent basis was capable of completely ameliorating EAE symptoms in mice, with none of the treated mice showing signs of paralysis throughout the 25-day study. This was in contrast to mice treated with mannitol or with free $PLP_{139-151}$, both of which experienced symptoms of paralysis. Additionally, mice treated with 4-arm $PLP_{139-151}$ also maintained a healthy weight

throughout the study (Figure 4), further supporting the efficacy associated with multivalent display of antigen.

Investigations into the phenotypic changes associated with the amelioration of EAE symptoms at peak of disease supported the role of B cell interactions in the efficacy of 4-arm $PLP_{139-151}$ treatment. Most notably, 72-hour *in vitro* treatment with 4-arm $PLP_{139-151}$ resulted in nearly complete depletion of $CD19^{+hi}$ cells (Figure 5), a B cell population which was highly enhanced in response to treatment with 25 μM free $PLP_{139-151}$. We postulate that these $CD19^{+hi}$ B cells are associated with EAE disease onset due to their prevalence following treatment with 25 μM free $PLP_{139-151}$. This is supported by literature indicating overexpression of CD19 in transgenic mice results in enhanced proliferative response to antigens and may result in a breakdown of peripheral tolerance, allowing autoreactive B cells to overcome anergy.[32–33] In addition, high avidity interactions between antigen and respective BCRs in the absence of secondary co-stimulatory signals are often associated with induction of B cell anergy, a state of immunological unresponsiveness.[34–37] Therefore, depletion of $CD19^{+hi}$ B cells specific to $PLP_{139-151}$ is likely a key mechanism by which 4-arm $PLP_{139-151}$ is capable of ameliorating EAE symptoms.

In addition to the depletion of $CD19^{+hi}$ B cells, 4-arm $PLP_{139-151}$ treatment also altered the expression of co-stimulatory markers CD80 and CD86. CD80 expression significantly increased following treatment with 4-arm $PLP_{139-151}$ both with and without the addition of 25 μM free $PLP_{139-151}$ (Figure 6A). Conversely, the expression of CD86 was significantly reduced when treated with 4-arm $PLP_{139-151}$ + 25 μM free $PLP_{139-151}$, in comparison to 25 μM free $PLP_{139-151}$ alone (Figure 6B). In order to interpret these results, it is important to first understand the role these co-stimulatory markers play with regards to T cell activation. Primarily expressed on antigen-presenting cells, the ligands CD80 and CD86 modulate T cell responses through binding to one of two receptors: CD28 or cytotoxic T lymphocyte-associated antigen 4 (CTLA-4). It has been demonstrated that the functions of these two ligands are distinct and opposing with regards to T cell activation.[38–41] Manzotti and colleagues found that ligation of CTLA-4 with CD86 was associated with T cell proliferation, whereas ligation of CTLA-4 with CD80 resulted primarily in inhibition of T cell activation.[38] Based on these data, a model was proposed in which CD80 preferentially interacts with CTLA-4 in the absence of inflammatory stimuli, restricting T cell activation.[41] Therefore, the resulting shift in CD80/CD86 expression observed in EAE splenocytes following treatment with 4-arm $PLP_{139-151}$ may inhibit the T cell response to PLP. A similar result has been observed in studies of soluble antigen arrays (SAgAs) at varying antigen valency, wherein the lowest valency SAgAs most strongly displayed an upregulation of CD80 and downregulation of CD86.[16] This effect was less pronounced as SAgA antigen valency was increased, suggesting low valency antigen arrays (e.g. <4–6 antigens per backbone) may have the greatest immunosuppressive effects, a result in agreement with the studies performed here.

In order to determine the effect of 4-arm $PLP_{139-151}$ treatment on T cell response, we quantified the expression of key inflammatory cytokines following *in vitro* treatment. Generally, only samples which included 25 μM free $PLP_{139-151}$ resulted in significant changes in cytokines (Figure 7). EAE splenocytes treated with 25 μM free $PLP_{139-151}$ alone

resulted in increased secretion of inflammatory cytokines such as IFN-γ, TNF-α, IL-2, IL-17A, and IL-6, clearly showing immune stimulation associated with $PLP_{139-151}$ rechallenge. Interestingly, splenocytes treated with 4-arm $PLP_{139-151}$ + 25 μM free $PLP_{139-151}$ expressed significantly lower levels of each of these inflammatory cytokines despite the inclusion of free, cognate antigen. In contrast, prior reports of multivalent SAgAs displaying $PLP_{139-151}$ showed increases of IL-17, TNF-α, and IL-6 in the presence of free antigen.[16] Thus, the 4-arm $PLP_{139-151}$ may be a more potent inhibitor of effector T cell activation in the presence of antigen rechallenge as compared to SAgAs; however, further studies directly comparing the two multivalent arrays are necessary to determine precisely how this difference is propagated to effector T cells. The proinflammatory cytokines studied here have been implicated in the onset of EAE and inhibiting their secretion may represent a shift away from pathogenic T helper subsets; however, further studies focused on T-cell response to 4-arm $PLP_{139-151}$ treatment will be necessary.[42–46]

5. Conclusions

The synthesis and characterization of a soluble tetrameric antigen display system was tested for the induction of antigen-specific tolerance. EAE was induced using $PLP_{139-151}$ and subsequently treated using the very same $PLP_{139-151}$ peptide or a ~25 kDa 4-arm $PLP_{139-151}$ construct designed to target and disarm pathogenic B cells specific to this epitope. The simple change to a 4-arm $PLP_{139-151}$ structure completely negated the development of EAE in contrast to treatment using the same dose of 'free' $PLP_{139-151}$ peptide. *In vitro* studies of 4-arm $PLP_{139-151}$ with EAE mouse splenocytes probed the mechanism and demonstrated that the therapeutic efficacy observed *in vivo* was likely the result of depletion of $PLP_{139-151}$-specific $CD19^{+hi}$ B cells. Depletion of CD19+hi B cells is consistent with our hypothesized mechanism of avidity-induced BCR crosslinking and sustained receptor occupancy leading to B cell disarmament. Furthermore, the mechanism was affirmed in splenocyte cultures containing free $PLP_{139-151}$, since the expected immune stimulation upon cognate antigen rechallenge was blocked by 4-arm $PLP_{139-151}$. Additionally, the overall expression of CD80, associated with preferential inhibition of T cells, was increased, while the expression of CD86, associated with T cell proliferation, was decreased. This indicated the 4-arm $PLP_{139-151}$ inhibited $PLP_{139-151}$-specific inflammatory responses and reduced activation of effector T cells. A reduction in numerous inflammatory cytokines in response to free $PLP_{139-151}$ further corroborated this trend. In summary, EAE was completely blocked in mice via antigen-specific disarmament of encephalogenic autoimmune cells when treated with a multivalent 4-arm $PLP_{139-151}$ version of the normally encephalogenic $PLP_{139-151}$ epitope.

Supplementary Material

Refer to Web version on PubMed Central for supplementary material.

Acknowledgements

References

1. Torkildsen O; Myhr KM; Bo L, Disease-modifying treatments for multiple sclerosis - a review of approved medications. Eur J Neurol 2016, 23 Suppl 1, 18–27. [PubMed: 26563094]

2. Jones JL; Coles AJ, New treatment strategies in multiple sclerosis. Exp Neurol 2010, 225 (1), 34–9. [PubMed: 20547155]

3. Boster A; Edan G; Frohman E; Javed A; Stuve O; Tselis A; Weiner H; Weinstock-Guttman B; Khan O, Intense immunosuppression in patients with rapidly worsening multiple sclerosis: treatment guidelines for the clinician. Lancet Neurol 2008, 7 (2), 173–83. [PubMed: 18207115]

4. Fletcher JM; Lalor SJ; Sweeney CM; Tubridy N; Mills KH, T cells in multiple sclerosis and experimental autoimmune encephalomyelitis. Clin Exp Immunol 2010, 162 (1), 1–11. [PubMed: 20682002]

5. Lehmann-Horn K; Kronsbein HC; Weber MS, Targeting B cells in the treatment of multiple sclerosis: recent advances and remaining challenges. Ther Adv Neurol Disord 2013, 6 (3), 161–73. [PubMed: 23634189]

6. Amor S; Puentes F; Baker D; van der Valk P, Inflammation in neurodegenerative diseases. Immunology 2010, 129 (2), 154–69. [PubMed: 20561356]

7. Bar-Or A; Calabresi PA; Arnold D; Markowitz C; Shafer S; Kasper LH; Waubant E; Gazda S; Fox RJ; Panzara M; Sarkar N; Agarwal S; Smith CH, Rituximab in relapsing-remitting multiple sclerosis: a 72-week, open-label, phase I trial. Ann Neurol 2008, 63 (3), 395–400. [PubMed: 18383069]

8. Hauser SL; Waubant E; Arnold DL; Vollmer T; Antel J; Fox RJ; Bar-Or A; Panzara M; Sarkar N; Agarwal S; Langer-Gould A; Smith CH, B-cell depletion with rituximab in relapsing-remitting multiple sclerosis. N Engl J Med 2008, 358 (7), 676–88. [PubMed: 18272891]

9. Kappos L; Li D; Calabresi PA; O'Connor P; Bar-Or A; Barkhof F; Yin M; Leppert D; Glanzman R; Tinbergen J; Hauser SL, Ocrelizumab in relapsing-remitting multiple sclerosis: a phase 2, randomised, placebo-controlled, multicentre trial. Lancet 2011, 378 (9805), 1779–87. [PubMed: 22047971]

10. Sorensen PS; Lisby S; Grove R; Derosier F; Shackelford S; Havrdova E; Drulovic J; Filippi M, Safety and efficacy of ofatumumab in relapsing-remitting multiple sclerosis: a phase 2 study. Neurology 2014, 82 (7), 573–81. [PubMed: 24453078]

11. Dintzis HM; Dintzis RZ; Vogelstein B, Molecular determinants of immunogenicity: the immunon model of immune response. Proceedings of the National Academy of Sciences 1976, 73 (10), 3671–3675.

12. Diao L; Meibohm B, Pharmacokinetics and Pharmacokinetic–Pharmacodynamic Correlations of Therapeutic Peptides. Clinical Pharmacokinetics 2013, 52 (10), 855–868. [PubMed: 23719681]

13. Richter WF; Bhansali SG; Morris ME, Mechanistic Determinants of Biotherapeutics Absorption Following SC Administration. The AAPS Journal 2012, 14 (3), 559–570. [PubMed: 22619041]

14. Reim JW; Symer DE; Watson DC; Dintzis RZ; Dintzis HM, Low molecular weight antigen arrays delete high affinity memory B cells without affecting specific T-cell help. Mol Immunol 1996, 33 (17–18), 1377–88. [PubMed: 9171897]

15. Hartwell BL; Pickens CJ; Leon M; Northrup L; Christopher MA; Griffin JD; Martinez-Becerra F; Berkland C, Soluble antigen arrays disarm antigen-specific B cells to promote lasting immune tolerance in experimental autoimmune encephalomyelitis. J Autoimmun 2018, 93, 76–88. [PubMed: 30007842]

16. Griffin JD; Leon MA; Salash JR; Shao M; Hartwell BL; Pickens CJ; Sestak JO; Berkland C, Acute B-Cell Inhibition by Soluble Antigen Arrays Is Valency-Dependent and Predicts

Immunomodulation in Splenocytes. Biomacromolecules 2019, 20 (5), 2115–2122. [PubMed: 30995843]

17. Leon MA; Wemlinger SM; Larson NR; Ruffalo JK; Sestak JO; Middaugh CR; Cambier JC; Berkland C, Soluble Antigen Arrays for Selective Desensitization of Insulin-Reactive B Cells. Mol Pharm 2019, 16 (4), 1563–1572. [PubMed: 30681867]

18. Sestak J; Mullins M; Northrup L; Thati S; Forrest ML; Siahaan TJ; Berkland C, Single-step grafting of aminooxy-peptides to hyaluronan: a simple approach to multifunctional therapeutics for experimental autoimmune encephalomyelitis. J Control Release 2013, 168 (3), 334–40. [PubMed: 23541930]

19. Hartwell BL; Martinez-Becerra FJ; Chen J; Shinogle H; Sarnowski M; Moore DS; Berkland C, Antigen-Specific Binding of Multivalent Soluble Antigen Arrays Induces Receptor Clustering and Impedes B Cell Receptor Mediated Signaling. Biomacromolecules 2016, 17 (3), 710–22. [PubMed: 26771518]

20. Johnson JG; Jemmerson R, Tolerance induction in resting memory B cells specific for a protein antigen. The Journal of Immunology 1992, 148 (9), 2682–2689. [PubMed: 1315356]

21. Linton PJ; Rudie A; Klinman NR, Tolerance susceptibility of newly generating memory B cells. The Journal of Immunology 1991, 146 (12), 4099–4104. [PubMed: 2040792]

22. Symer DE; Reim J; Dintzis RZ; Voss EW; Dintzis HM, Durable elimination of high affinity, T cell-dependent antibodies by low molecular weight antigen arrays in vivo. The Journal of Immunology 1995, 155 (12), 5608–5616. [PubMed: 7499844]

23. Miyagaki T; Fujimoto M; Sato S, Regulatory B cells in human inflammatory and autoimmune diseases: from mouse models to clinical research. Int Immunol 2015, 27 (10), 495–504. [PubMed: 25957264]

24. McRae BL; Miller SD, Fine specificity of CD4+ T cell responses to the dominant encephalitogenic PLP 139–151 peptide in SJL/J mice. Neurochem Res 1994, 19 (8), 997–1004. [PubMed: 7528357]

25. Luca ME; Kel JM; van Rijs W; Wouter Drijfhout J; Koning F; Nagelkerken L, Mannosylated PLP(139–151) induces peptide-specific tolerance to experimental autoimmune encephalomyelitis. J Neuroimmunol 2005, 160 (1–2), 178–87. [PubMed: 15710471]

26. Kobayashi N; Kobayashi H; Gu L; Malefyt T; Siahaan TJ, Antigen-specific suppression of experimental autoimmune encephalomyelitis by a novel bifunctional peptide inhibitor. J Pharmacol Exp Ther 2007, 322 (2), 879–86. [PubMed: 17522343]

27. Wegmann KW; Wagner CR; Whitham RH; Hinrichs DJ, Synthetic Peptide dendrimers block the development and expression of experimental allergic encephalomyelitis. J Immunol 2008, 181 (5), 3301–9. [PubMed: 18714002]

28. Choi CHJ; Zuckerman JE; Webster P; Davis ME, Targeting kidney mesangium by nanoparticles of defined size. Proceedings of the National Academy of Sciences 2011, 108 (16), 6656–6661.

29. Saffer EM; Lackey MA; Griffin DM; Kishore S; Tew GN; Bhatia SR, SANS study of highly resilient poly(ethylene glycol) hydrogels. Soft Matter 2014, 10 (12), 1905–1916. [PubMed: 24652367]

30. Sosnick TR; Benjamin DC; Novotny J; Seeger PA; Trewhella J, Distances between the antigen-binding sites of three murine antibody subclasses measured using neutron and X-ray scattering. Biochemistry 1992, 31 (6), 1779–86. [PubMed: 1737031]

31. Reth M, Matching cellular dimensions with molecular sizes. Nat Immunol 2013, 14 (8), 765–7. [PubMed: 23867923]

32. Fujimoto M; Poe JC; Inaoki M; Tedder TF, CD19 regulates B lymphocyte responses to transmembrane signals. Semin Immunol 1998, 10 (4), 267–77. [PubMed: 9695183]

33. Engel P; Zhou L-J; Ord DC; Sato S; Koller B; Tedder TF, Abnormal B lymphocyte delevopment, activation, and differentiation in mice that lack or overexpress the CD19 signal transduction molecule. Immunity 1995, 3 (1), 39–50. [PubMed: 7542548]

34. Parker DC, T Cell-Dependent B Cell Activation. Annual Review of Immunology 1993, 11 (1), 331–360.

35. Gauld SB; Benschop RJ; Merrell KT; Cambier JC, Maintenance of B cell anergy requires constant antigen receptor occupancy and signaling. Nat Immunol 2005, 6 (11), 1160–7. [PubMed: 16200069]

36. Hartwell BL; Pickens CJ; Leon M; Berkland C, Multivalent Soluble Antigen Arrays Exhibit High Avidity Binding and Modulation of B Cell Receptor-Mediated Signaling to Drive Efficacy against Experimental Autoimmune Encephalomyelitis. Biomacromolecules 2017, 18 (6), 1893–1907. [PubMed: 28474886]

37. Yarkoni Y; Getahun A; Cambier JC, Molecular underpinning of B-cell anergy. Immunol Rev 2010, 237 (1), 249–263. [PubMed: 20727040]

38. Manzotti CN; Tipping H; Perry LC; Mead KI; Blair PJ; Zheng Y; Sansom DM, Inhibition of human T cell proliferation by CTLA-4 utilizes CD80 and requires CD25+ regulatory T cells. Eur J Immunol 2002, 32 (10), 2888–96. [PubMed: 12355442]

39. Zheng Y; Manzotti CN; Liu M; Burke F; Mead KI; Sansom DM, CD86 and CD80 differentially modulate the suppressive function of human regulatory T cells. J Immunol 2004, 172 (5), 2778–84. [PubMed: 14978077]

40. Nova-Lamperti E; Fanelli G; Becker PD; Chana P; Elgueta R; Dodd PC; Lord GM; Lombardi G; Hernandez-Fuentes MP, IL-10-produced by human transitional B-cells down-regulates CD86 expression on B-cells leading to inhibition of CD4+T-cell responses. Sci Rep 2016, 6, 20044–20044. [PubMed: 26795594]

41. Sansom DM; Manzotti CN; Zheng Y, What's the difference between CD80 and CD86? Trends in Immunology 2003, 24 (6), 313–318.

42. Arellano G; Ottum PA; Reyes LI; Burgos PI; Naves R, Stage-Specific Role of Interferon-Gamma in Experimental Autoimmune Encephalomyelitis and Multiple Sclerosis. Front Immunol 2015, 6, 492–492. [PubMed: 26483787]

43. Hofman FM; Hinton DR; Johnson K; Merrill JE, Tumor necrosis factor identified in multiple sclerosis brain. The Journal of experimental medicine 1989, 170 (2), 607–12. [PubMed: 2754393]

44. Ruddle NH; Bergman CM; McGrath KM; Lingenheld EG; Grunnet ML; Padula SJ; Clark RB, An antibody to lymphotoxin and tumor necrosis factor prevents transfer of experimental allergic encephalomyelitis. The Journal of experimental medicine 1990, 172 (4), 1193–200. [PubMed: 2212948]

45. Komiyama Y; Nakae S; Matsuki T; Nambu A; Ishigame H; Kakuta S; Sudo K; Iwakura Y, IL-17 plays an important role in the development of experimental autoimmune encephalomyelitis. J Immunol 2006, 177 (1), 566–73. [PubMed: 16785554]

46. Serada S; Fujimoto M; Mihara M; Koike N; Ohsugi Y; Nomura S; Yoshida H; Nishikawa T; Terabe F; Ohkawara T; Takahashi T; Ripley B; Kimura A; Kishimoto T; Naka T, IL-6 blockade inhibits the induction of myelin antigen-specific Th17 cells and Th1 cells in experimental autoimmune encephalomyelitis. Proceedings of the National Academy of Sciences 2008, 105 (26), 9041–9046.
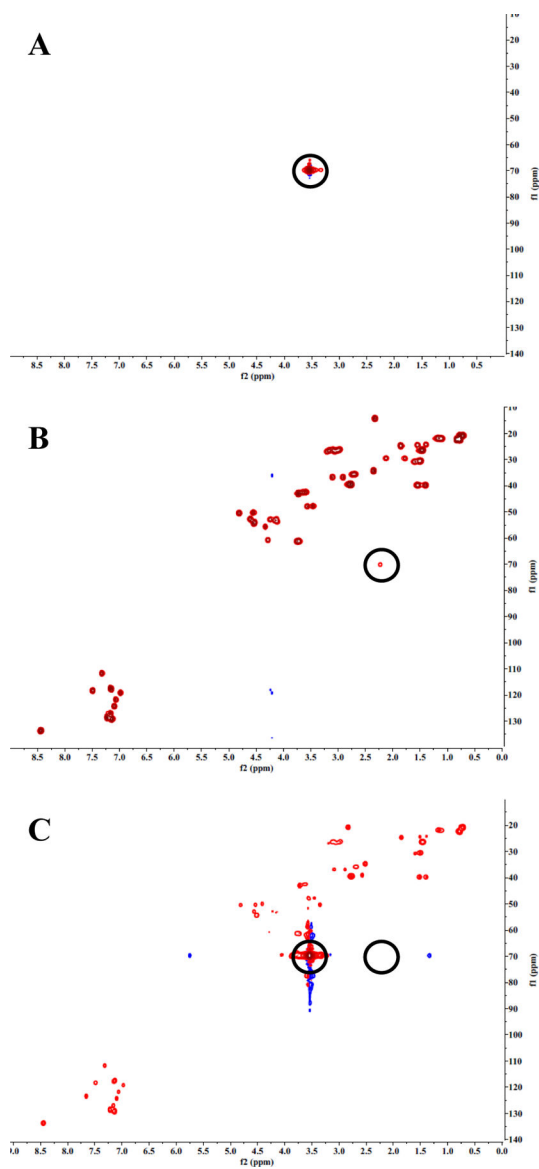
Figure 1.
HSQC NMR spectra of 20 kDa 4-arm PEG-azide (A), hpPLP$_{139-151}$ (B), and 4-arm PLP$_{139-151}$ (C). hpPLP$_{139-151}$ (B) shows a unique resonance from the alkyne peak. 4-arm PLP$_{139-151}$ (C) does not show the resonance from the alkyne peak, indicating that no residual unconjugated PLP$_{139-151}$ is present in the final product.

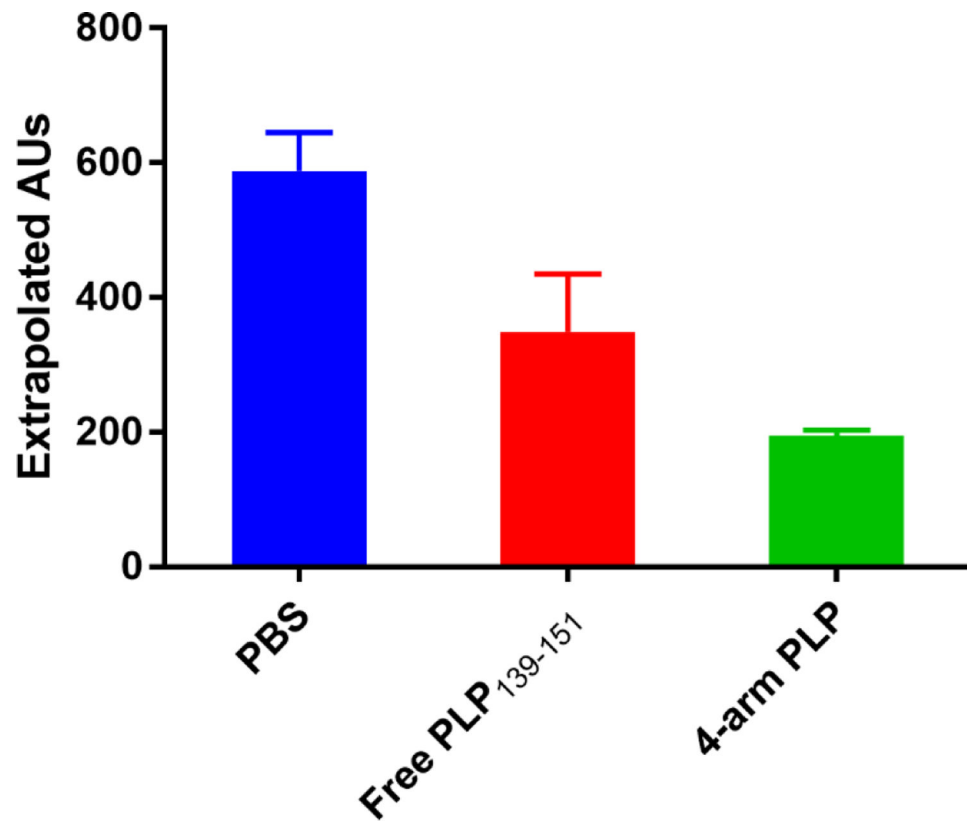**Figure 2.**
PLP$_{139-151}$-specific IgG antibody titers in EAE mouse serum detected by ELISA following one hour serum incubation with (A) PBS vehicle control (B) Free PLP$_{139-151}$ and (C) 4-arm PLP$_{139-151}$.
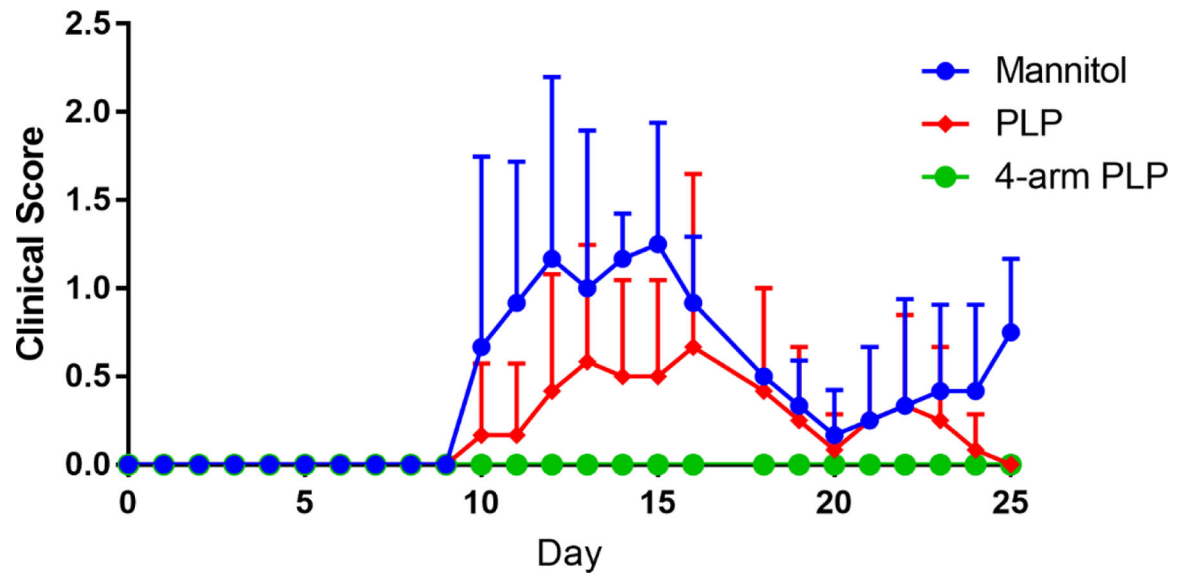
Figure 3.
Clinical scores of EAE mice treated *in vivo* with (A) free $PLP_{139-151}$ and (B) 4-arm $PLP_{139-151}$. Treatments were administered subcutaneously on days 4, 7, and 10 with 40 mg/mL mannitol as vehicle. All doses were based on 200 nmol $PLP_{139-151}$ basis. N=6 for all groups. Data is presented as mean ± SD.
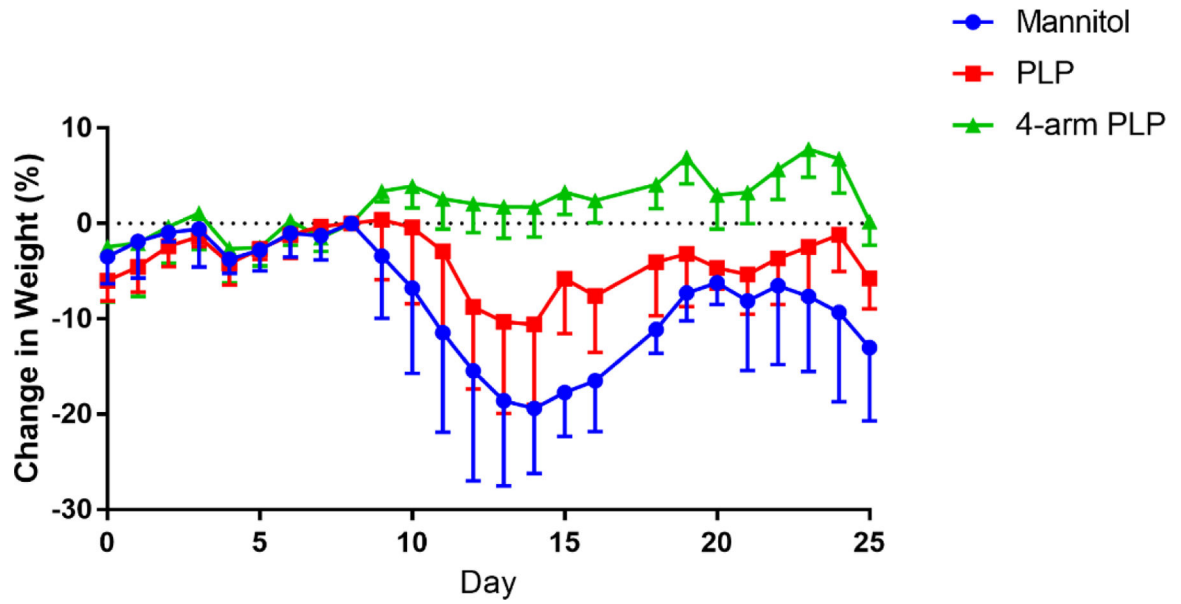
Figure 4.
Animal weight data of EAE mice treated *in vivo* with (A) free PLP$_{139-151}$ and (B) 4-arm PLP$_{139-151}$. Treatments were administered subcutaneously on days 4, 7, and 10 with 40 mg/mL mannitol as vehicle. All doses were based on 200 nmol PLP$_{139-151}$ basis. N=6 for all groups. Data is presented as mean ± SD of % change in weight normalized to mouse weight at day 8.
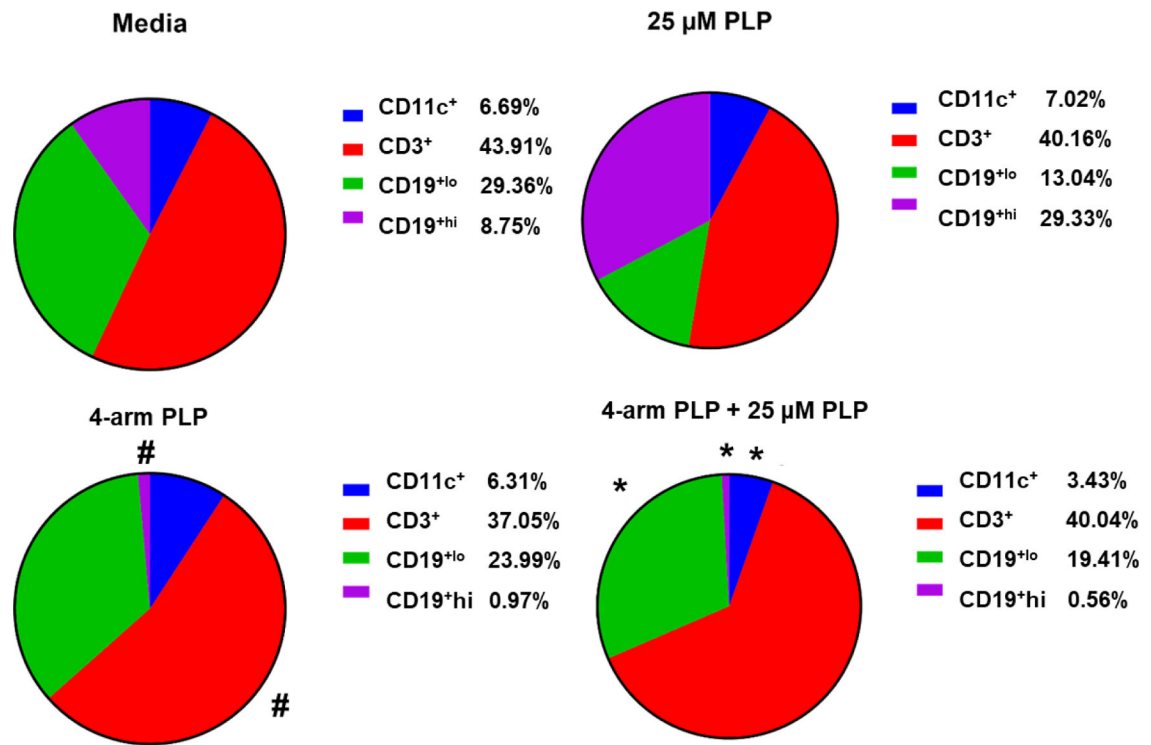
Figure 5.

Percent of total singlet splenocytes expressing CD11c, CD3, CD19^{lo}, and CD19^{hi} following *in vitro* incubation for 72 hours with media, 25 μM free PLP$_{139-151}$, 4-arm PLP$_{139-151}$, and 4-arm PLP$_{139-151}$ + 25 μM free PLP$_{139-151}$. Data is presented as mean ± SD. N=3, * represents significance from 25 μM free PLP$_{139-151}$. # represents significance from Media.
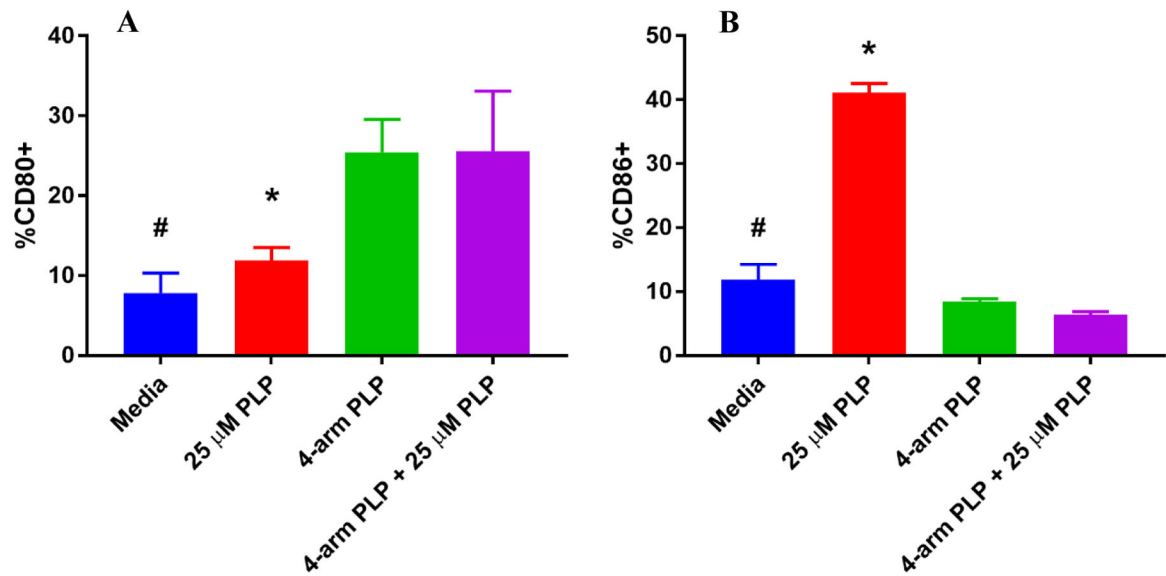
Figure 6.
Percent of total singlet splenocytes expressing (A) CD80 and (B) CD86 following *in vitro* incubation for 72 hours with (I) media (II) 25 μM free PLP$_{139-151}$ (III) 4-arm PLP$_{139-151}$ and (IV) 4-arm PLP$_{139-151}$ + 25 μM free PLP$_{139-151}$. Data is presented as mean ± SD. N=3, * represents significance from 4-arm PLP$_{139-151}$ + 25 μM free PLP$_{139-151}$. # represents significance from 4-arm PLP$_{139-151}$.
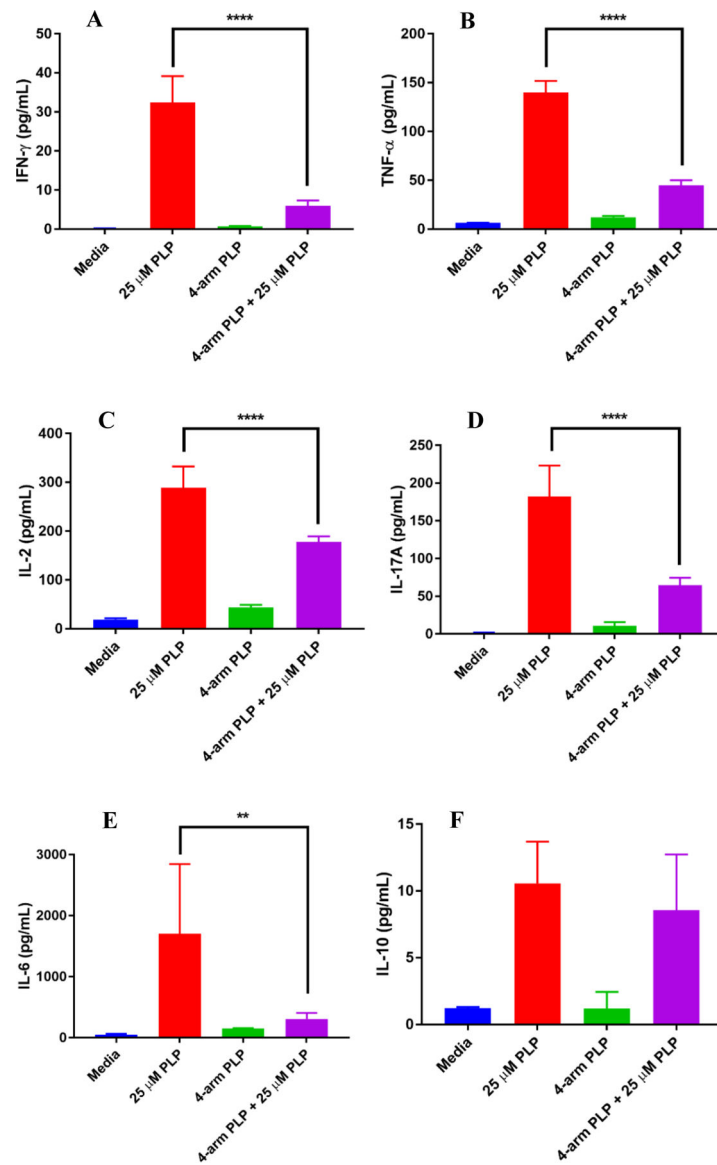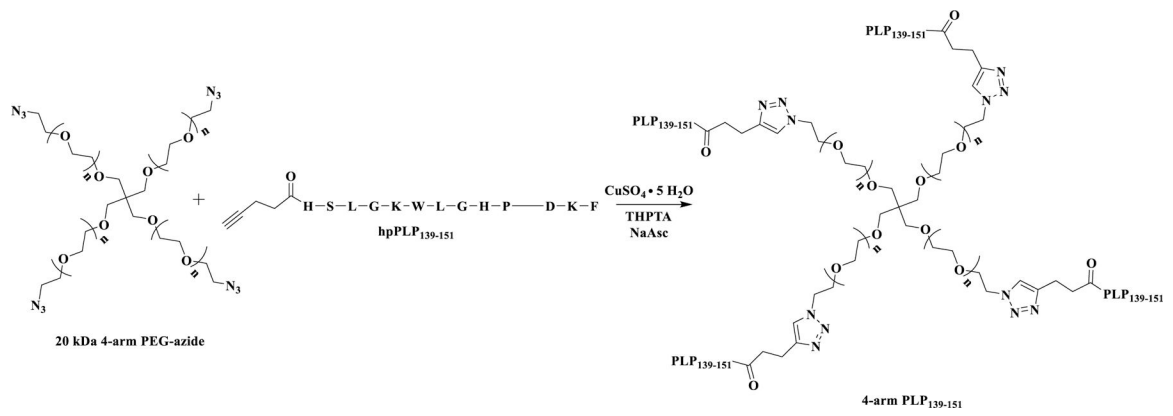
Figure 7.
Concentrations of (A) IFN-γ (B) TNF-α (C) IL-2 (D) IL-17A (E) IL-6 and (F) IL-10 following 72 hr *in vitro* incubation with (I) media (II) 25 μM free $PLP_{139-151}$ (III) 4-arm $PLP_{139-151}$ and (IV) 4-arm $PLP_{139-151}$ + 25 μM free $PLP_{139-151}$. Data is presented as mean ± SD. N=3, * p<0.05, ** p<0.01, *** p<0.001, **** p<0.0001.

Scheme 1.
Reaction scheme for the synthesis of 4-arm PLP$_{139-151}$.

Table 1.

Size information for hpPLP$_{139-151}$, 20 kDa 4-Arm PEG-azide, and 4-arm PLP$_{139-151}$ from SEC, DLS, and MALDI-TOF analysis.

	Size by SEC (Da)	Size by DLS (nm)	Size by MALDI-TOF (Da)
hpPLP$_{139-151}$	n.d.	n.d.	1,602
20 kDa 4-arm PEG-N$_3$	26,940	1.7 ± 0.14	20,367
4-arm PLP$_{139-151}$	28,940	1.8 ± 0.15	23,748